Detecting nanoscale distribution of protein pairs by proximity-dependent super-resolution microscopy

Tobias Lutz [†], William T. Kaufhold [‡], Alexander H. Clowsley [†], Anna Meletiou [†], Lorenzo Di Michele [‡], Christian Soeller *[,†]

[†]Living Systems Institute & Biomedical Physics, University of Exeter, Exeter, UK

[‡]Cavendish Laboratory, University of Cambridge, Cambridge, UK

Super-resolution microscopy, DNA-PAINT, proximity assay, DNA nanotechnology, proximity-mediated strand displacement

ABSTRACT: Interactions between biomolecules such as proteins underlie most cellular processes. It is crucial to visualize these molecular-interaction complexes directly within the cell, to show precisely where these interactions occur and thus improve our understanding of cellular regulation. Currently available proximity-sensitive assays for in situ imaging of such interactions produce diffraction-limited signals and therefore preclude obtaining information on the nanometer-scale distribution of interaction complexes. By contrast, optical super-resolution imaging provides information about molecular distributions with nanometer resolution which has greatly advanced our understanding of cell biology. However, current colocalization analysis of super-resolution fluorescence imaging is prone to false positive signals as the detection of protein proximity is directly dependent on the local optical resolution. Here we present Proximity-Dependent PAINT (PD-PAINT), a method for sub-diffraction imaging of protein pairs, in which proximity detection is decoupled from optical resolution. Proximity is detected via the highly distance-dependent interaction of two DNA labels anchored to the target species. Labelled protein pairs are then imaged with high contrast and nanoscale resolution using the super-resolution approach of DNA-PAINT. The mechanisms underlying the new technique are analyzed by means of coarse-grained molecular simulations and experimentally demonstrated by imaging high proximity biotin binding sites of streptavidin and epitopes of ryanodine receptor proteins in cardiac tissue samples. We show that PD-PAINT can be straightforwardly integrated in a multiplexed super-resolution imaging protocol and benefits from advantages of DNA-based super-resolution localization microscopy, such as high specificity, high resolution and the ability to image quantitatively.

Introduction. Characterizing protein interactions by detection of protein-protein complexes is the basis of understanding many processes in biology [1]. Often, these are detected by in vitro methods such as co-immunoprecipitation, cross-linking or affinity blotting [2,3]. It is increasingly evident that besides detecting the mere presence of protein-protein interactions, it is important to determine where these occur within a cell or tissue, since the nanoscale organization of signaling complexes directly controls cell function [4,5]. To this end, methods have been developed that are based on labelling the features of interest with synthetic DNA oligonucleotides, conjugated to antibodies or other molecular markers. The oligonucleotides act as proximity probes, and a subsequent amplification step is implemented to produce a fluorescent signal detectable by a conventional microscope. In an (in situ*) proximity ligation assay* (PLA), enzymatic amplification occurs via the rolling circle method [5–8], while in the ProxHCR scheme amplification is non-enzymatic and relies on a hybridization chain reaction [9,10]. However, the high fluorescent amplification in both methods also effectively restricts them to diffraction-limited imaging. This implies that the presence of protein pairs can be located to within a certain region but generally precludes accurate quantification and visualization of their distribution at the nanometer scale [11].

Imaging with spatial resolution beyond the diffraction limit can now be achieved by a wide range of super-resolution techniques, such as structured illumination microscopy (SIM) [12], stimulated emission depletion (STED) microscopy [13,14], (fluorescence) photoactivated localization microscopy ((F)PALM) [15,16] or (direct) stochastic optical reconstruction microscopy ((d)STORM) [17,18]. DNA-PAINT (Point Accumulation Imaging in Nanoscale Topography) is a super-resolution imaging technique that relies on oligonucleotide interactions, a property that it shares with PLA and proxHCR [19]. In DNA-PAINT, the proteins of interest are labelled with a short DNA oligonucleotide, or "docking" strand. The transient binding and consequent brief immobilization of fluorescently labeled complementary "imager" strands enables detection as a fluorescent "blink" and precise localization. The accumulated localization data is used to reconstruct a super-resolution image.

Fluorescent super-resolution techniques can be used to acquire multi-target images which, in principle, allow estimating the proximity of protein targets by fluorescence colocalization. However, unequivocal identification of protein-protein pairs is complicated by the fact that co-localization can be prone to false-positive signals, as the precision of colocalization is directly dependent on the local imaging resolution. Resolution can vary considerably, especially in optically complex samples such as thick cells or tissue sections. Often, there is limited resolution along the optical axis (several hundreds of nanometers in 2D super-resolution techniques, >40 nm in 3D methods [20]) which can lead to additional false positives. Furthermore, registration errors between multiple channels, e.g. due to chromatic aberrations or sample drift, can lead to incorrect co-localization estimates.

Here, we introduce a proximity-sensitive super-resolution imaging method which allows detection of the presence and characterization of the local density and nanoscale distribution of protein-protein complexes, determining the detailed structure and morphology of possible clusters. Importantly, the proximity detection is fully decoupled from local imaging resolution and optical multi-channel registration is not required. In our approach, two proteins of interest are labelled with DNA constructs, which are designed to interact if in molecular proximity, and as a result allow for a DNA-PAINT signal to be detected. One

construct includes the DNA-PAINT docking sequence, which however is protected by a stable DNA stem loop structure, rendering the docking site effectively inaccessible. If the second target is within a distance of approximately 10 nm, the second DNA construct associated with it can displace the stem of the hairpin, thereby unfolding the loop, fully exposing the docking site, and enabling DNA-PAINT imaging of the structure. We term this new approach *Proximity-Dependent PAINT* (PD-PAINT) and demonstrate it by means of coarse-grained molecular simulations and experimentally by imaging high-proximity biotin binding sites on streptavidin and epitopes on cardiac ion channels. PD-PAINT combines proximity detection with all the advantages of DNA-PAINT. These include high specificity, straightforward implementation on a conventional fluorescence microscope, freedom in the choice of dye and wavelength and importantly the possibility of readily achieving high photon yields, resulting in very high resolution [19,21]. In addition, by exploiting the principle of quantitative PAINT (qPAINT), PD-PAINT enables accurate determination of the local density of protein pairs in the sample [19,22]. Finally, PD-PAINT is fully compatible with multi-color imaging and can be implemented in addition to conventional DNA-PAINT of multiple other channels, essentially without performance penalty. This is demonstrated here by following an Exchange-PAINT protocol [23], to image the protein complex as well as the individual protein epitopes in separate channels.

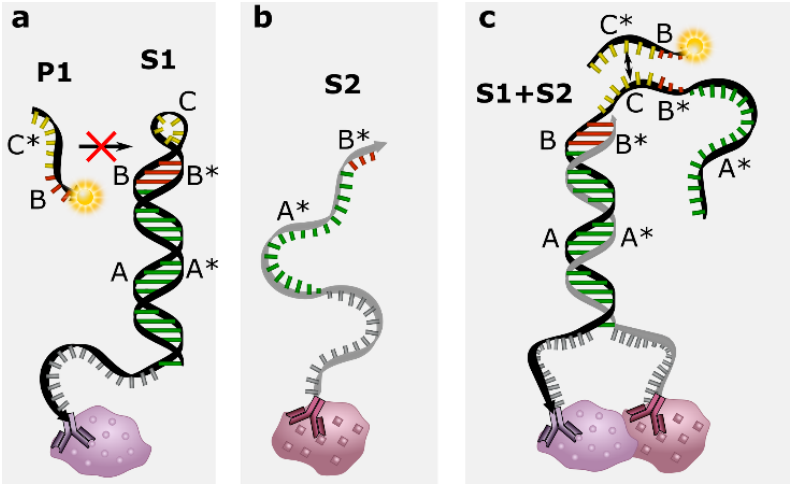

Figure 1. Principle of Proximity-Dependent PAINT (PD-PAINT). **a:** Strand S1 forms a stem loop structure which prevents imagers (P1) binding to the docking domain (B*C), due to a high curvature of domain S1-C and hybridization of domain S1-B* to S1-B. **b:** Strand S2 contains domains A* and B* which are complementary to A and B of the S1 stem. **c:** Close proximity of S1 and S2 allows the S2-A* domain to displace S1-A*, opening up the loop. The equilibrium probability and kinetics of the displacement is highly dependent on the distance between S1 and S2. The exposed docking domain in the open loop allows the transient binding of an imager to the S1-S2 complex so that a super-resolution image can be obtained by DNA-PAINT.

Results and Discussion. Fig. 1 demonstrates the principle of PD-PAINT, where fluorescence signals are only detected if two epitopes of interest are within close distance to each other. To implement PD-PAINT the two targets are labelled with oligonucleotides S1 and S2, e.g. via two types of antibody to which S1 and S2 are conjugated, respectively. As shown in Fig. 1a, S1 contains the 9 nt docking sequence consisting of domains B* (3 nt) and C (6 nt). When S1 is isolated, the docking site is protected by a closed stem-loop motif in which B* is hybridized to the complementary domain B, and C is wrapped to form a short loop. The loop is further stabilized by the complementary domains A and A* (17 bp). In the closed-loop configuration of S1 the docking site has negligible affinity for imagers of sequence C*-B (Fig. 1a), as previously determined in the context of catalytic DNA reactions [9] and further demonstrated by means of coarse-grained computer simulations discussed below. The second target is labelled with strand S2, which contains sequence A*-B* (Fig. 1b). This sequence is complementary to B-A in the S1 stem, making the S1-S2 dimerization reaction, and the consequent opening of the stem loop on S1, thermodynamically feasible only for sufficiently high concentrations of the constructs. If the local concentration of S1 and S2 is too low, e.g. ~500 nM used for sample labelling steps, the closed-loop configuration remains favorable. Furthermore, owing to the stability of the S1 stem, the dimerization reaction is kinetically highly unlikely unless the two species are kept in close proximity.

If S1 and S2 are attached to stationary epitopes located within close distance to each other, their dimerization can proceed through the process of *proximity-mediated strand displacement* (PMSD) [24,25]. Here, the occasional fraying taking place at either end of the S1 stem duplex enables the formation of transient base-pairing bonds with either the A* or the B* domains on S2, which then have a chance of progressing until S1 and S2 are fully hybridized through a stochastic branch-migration process [26]. The likelihood for the branch-migration to initiate, and thus the overall S1-S2 hybridization rate, is proportional to the local concentration of S1 and S2 and, as such, strongly proximity dependent [24,25]. Likewise, the equilibrium probability of the S1-S2 complex being formed is expected to depend on the distance between the tethered constructs. When S1 and S2 are fully hybridized the open loop exposes the docking sequence B*-C of S1, allowing transient binding of the complementary imager P1, which results in frequent detection of these binding events as fluorescent blinks, i.e., a DNA-PAINT signal (Fig. 1c).

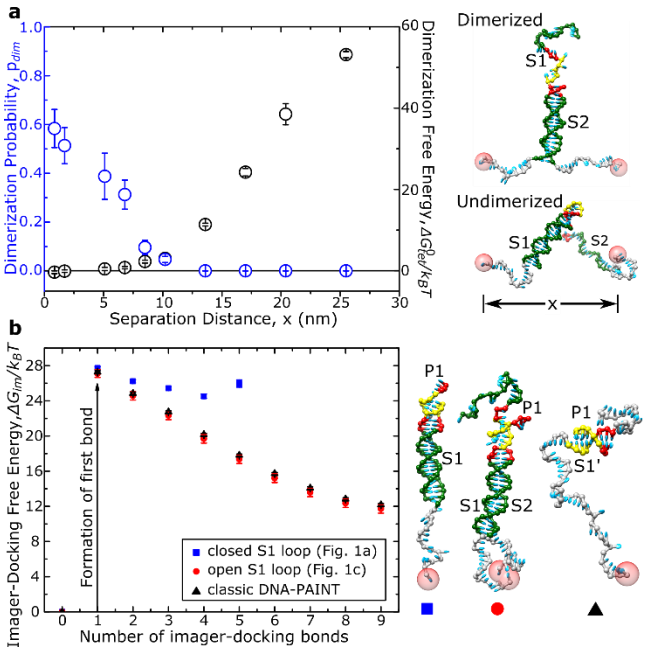

Figure 2. Thermodynamic properties of PD-PAINT. **a:** The dimerization probability of S1 and S2 is highly sensitive to the separation distance between tethers, *x*. Left: dimerization probabilities (blue) and the free energy change of dimerization (black) are calculated from coarse-grained Monte Carlo (MC) simulations based on the oxDNA model [27,28]. When the tethers are separated by short distances (1 nm), S1 and S2 dimerize with probability 0.6, forming a complex that can be imaged by DNA-PAINT. As separation distances increase the dimerization probability falls until dimerization is negligible at separation distances exceeding 10 nm. Right: simulation snapshots of the dimerized and undimerized configurations. **b:** Hybridization of the imager to S1 as a closed loop is inhibited in the absence of S2 and restored by the presence of S2. Left: free energy profiles for formation of Watson-Crick bonds between the imager and S1, relative to the unhybridized state. We compare the closed loop state of S1 (blue squares), the open state after hybridization of S2 (red circles) and conventional DNA-PAINT binding (black crosses). Note that closed loop states with >5 bonds resulted in large free energies whose contribution to the overall hybridization free energy is negligible. Right: simulation snapshots for the three cases. All DNA sequences used are shown in Table S1. Snapshots from the simulation are visualized with UCSF Chimera [29]. All errorbars are given as one standard error.

To explore the functionality of the proposed PD-PAINT scheme we investigated its thermodynamic properties by means of Monte Carlo (MC) simulations using the oxDNA coarse-grained model of nucleic acids, as described in details in the Supporting Information [27,28]. For PD-PAINT to elucidate the presence of dimers, it must obey two thermodynamic design criteria. First, the S1 loop must be opened if S2 is nearby. Second, binding of the imager to the closed loop must be inhibited to prevent false positives, i.e. binding should only be possible when the loop is open.

We implemented free-energy calculations to determine the likelihood of the formation of S1-S2 dimers, resulting in the opening of the S1 loop, as a function of the distance between their anchoring points (Fig. 2a). The standard free energy for S1-S2 dimerization and loop opening, with the strands tethered at distance *x* from each other, can be expressed as

$$\Delta G_{\text{tet}}(x) = \Delta G^0_{\text{sol}} - \phi^0(x)$$

where ΔG^0_{sol} is the standard free energy for dimerization of untethered S1 and S2, which can be estimated via nearest-neighbors thermodynamic rules for known S1 and S2 sequences [30], and $\phi^0(x)$ is a correction that encodes the free-energy cost of mutual confinement of the constructs following dimerization [31,32]. The latter is obtained from MC simulations and accounts for the polymer elasticity of the ssDNA segments (here 15 nt) connecting the active domains of S1 and S2 to their tethering points as well as excluded volume and electrostatic interactions between the constructs. As expected, both $\Delta G_{\text{tet}}(x)$ and the loop-opening probability, $p_{\text{dim}}(x)$, display a strong dependence on *x*, and $p_{\text{dim}}(x)$ effectively becomes negligible for distances exceeding ~10 nm (Fig. 2a). At small *x*, the loop-opening probability saturates at ~0.6 reflecting the fact that in conditions of high proximity a significant fraction of neighboring S1-S2 pairs will produce available docking sites. Note that once an ensemble of constructs is brought to a certain level of proximity, relaxation of the dimerization probability to the predicted distribution is not instantaneous, but will occur at a finite and separation-dependent rate, as well characterized for analogous PMSD processes [24,25]. It is therefore critical in experiments to allow sufficient time for the S1-S2 pairs to reach equilibrium. The dimerization probability for untethered constructs at a concentration of 500 nM, which was the maximal concentration used during sample functionalization steps, is $\sim 5.6 \times 10^{-4}$, implying that false positive signals resulting from the dimerization of untethered S1 and S2 should be negligible. The likelihood of this occurring on experimental timescales is further suppressed by the slow initiation kinetics of the branch migration process for freely diffusing constructs [24,25].

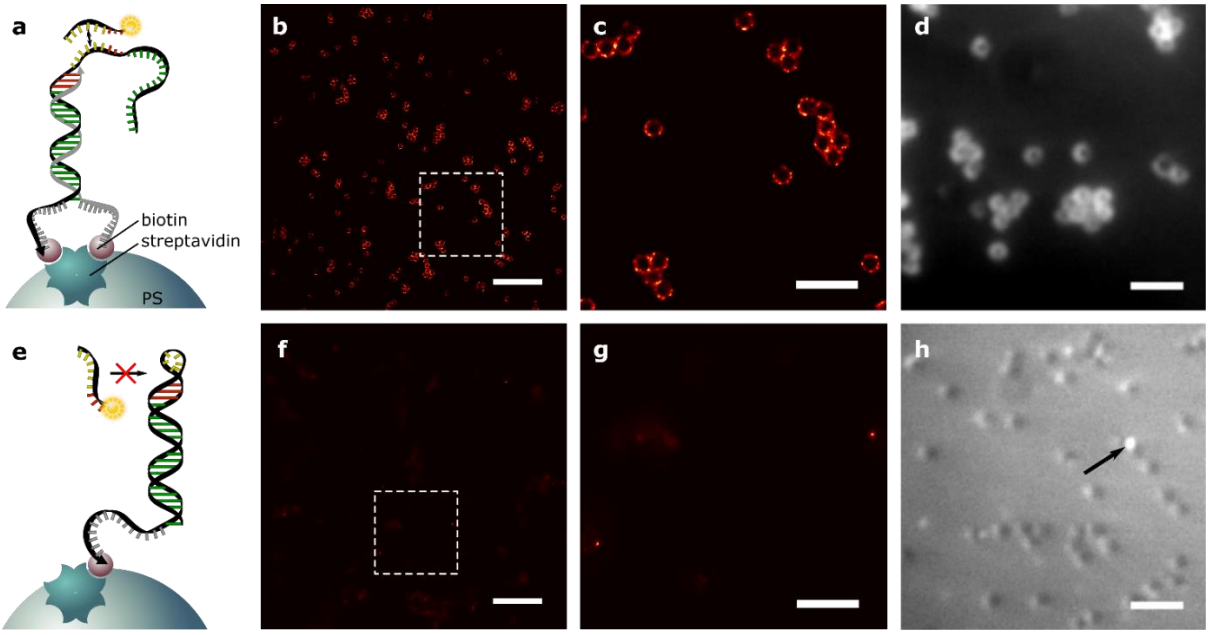

Figure 3. PD-PAINT to detect proximity of biotin binding sites on streptavidin. **a:** Biotinylated strands S1 and S2 were allowed to attach in equal amounts to the surface of streptavidin-coated 500 nm polystyrene spheres, which allows a considerable fraction of S2 to open up the S1 stem loop structure, whenever S1 and S2 attach to adjacent binding sites on the same protein. **b:** Rendered image of the resulting DNA-PAINT signal, the box indicates area of magnified inset in **c**. **d:** Widefield fluorescence image at high imager concentrations (5 nM), with many of the accessible docking domains occupied by imagers. **e:** If only S1 is used, the loop remains closed and does not allow imagers to bind. **f, g:** Rendered images, analogous to **b** and **c**, but displaying little signal. **h:** Widefield fluorescence image showing only a diffuse background fluorescence signal from comparatively high concentration of imagers (10 nM) in solution, outlining shadows of particles against the fluorescent background and very rare binding of single imagers (arrow). Note that the gray scale in **h** is different from **d**. Scale bars: 6 µm (b,f), 2 µm (c,d,g,h).

For the presence and location of S1-S2 dimers to be positively identified via DNA-PAINT, binding of the imager to closed S1 loops must be inhibited, yet the imager must have a sufficient affinity for the exposed docking site. We verify this by estimating the interaction free-energy $\Delta G_{\text{S1-P1}}$ between the P1 imager and S1 in its closed loop and open loop states, shown in Fig. 2b as a function of the number of formed base-pairing bonds. The free energy barrier for the formation of the first bond is similar between the open and closed loop configurations but while in the former case further base pairing does not result in a significant drop in free energy, a steep monotonic decrease is observed for the open-loop configuration. As a result, we estimate imager binding times to the closed S1 loop as ~1.4 µs, well below the detection threshold for a typical DNA PAINT experiment (see Supporting Information and Table S4). In turn, for the open loop configuration we predict a binding time of ~0.2 s, ideal for DNA-PAINT at typical frame integration times of 50-300 ms (Table S4). For comparison Fig. 2b also features the $\Delta G_{\text{S1-P1}}$ profile for a conventional DNA-PAINT docking strand that matches, within statistical errors, with the one determined for the open S1 construct.

To experimentally validate the PD-PAINT concept we used the biotin-binding sites of streptavidin as a well-studied model system that is expected to yield a positive PD-PAINT signal (Fig. 3). Streptavidin binds up to four biotin molecules, with two sites each located on either side of the protein tetramer, at a distance of ~2 nm from each other [33]. The very high affinity of biotin ensures an effectively permanent attachment of biotinylated S1 and S2 constructs. Streptavidin was attached to the surface of polystyrene colloidal particles, to provide a convenient imaging geometry as previously used in the context of DNA-PAINT by ourselves [34] and others [35]. Biotinylated S1 and S2 constructs were mixed thoroughly before streptavidin-coated particles were dispersed on the coverslip to ensure a stochastic attachment of S1 and S2 to the biotin-binding sites. The prominent ring structure observed in an optical section through the particles, shown in Fig. 3b,c, arises from a distinct PD-PAINT signal, providing positive confirmation that binding of DNA-PAINT imagers is observed as expected. Assuming a distance of ~2 nm between the anchoring points of S1 and S2, at equilibrium approximately 50% of these site-pairs should feature dimerized strands with an open S1 loop, as discussed above (Fig. 2a). DNA-PAINT imaging resulting in the super-resolved micrographs in Fig. 3b,c is performed at very low imager concentration (~0.05 nM), to reduce the likelihood of simultaneous binding events that would prevent single-molecule localization [19]. When imagers are added at a much higher concentration (5 nM), as shown in Fig. 3d, multiple docking sites within a diffraction-limited area are occupied, resulting in a fluorescence signal clearly visible in widefield fluorescence mode, consistent with a large fraction of all S1 loops being open and available for imager binding.

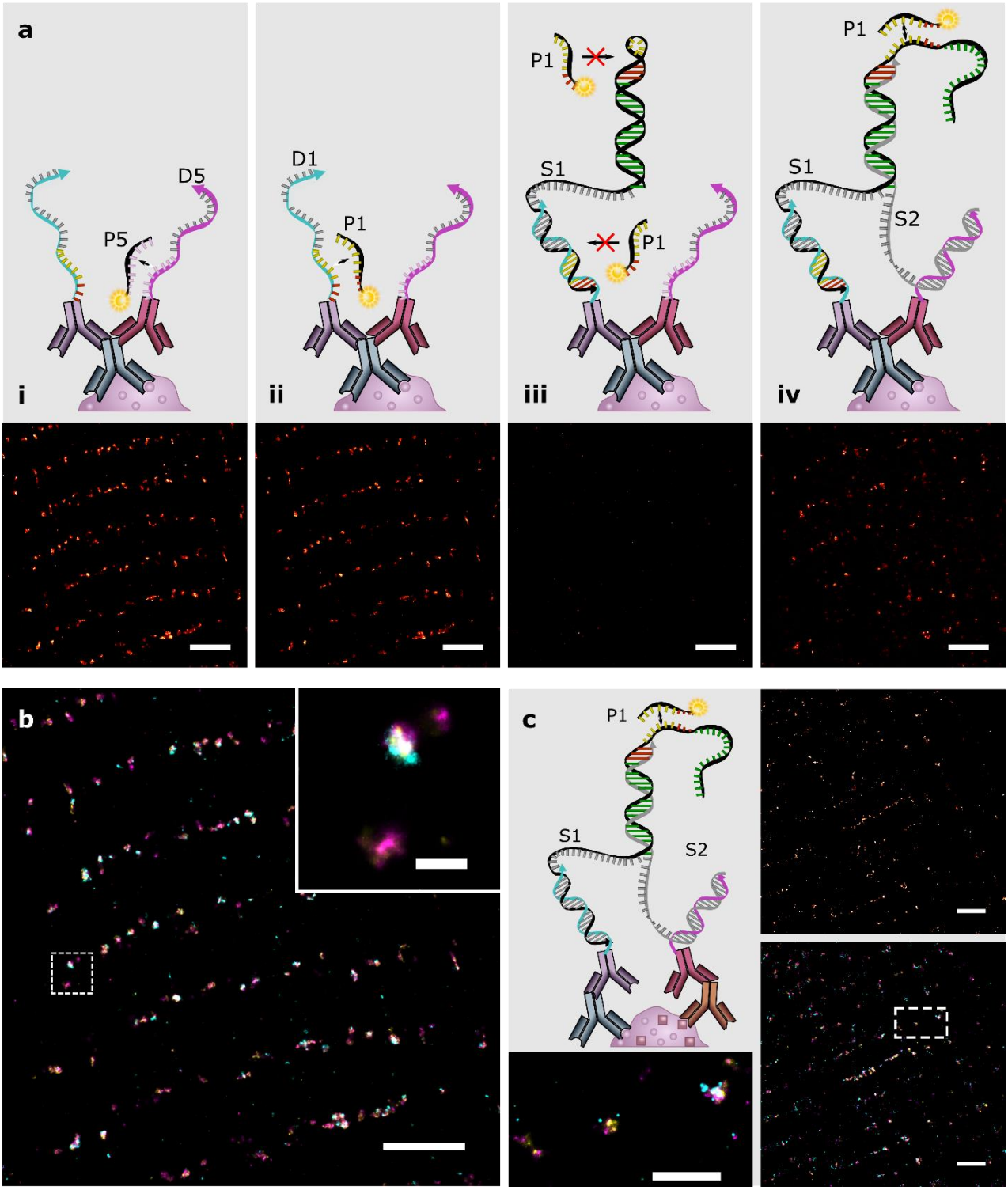

Figure 4. PD-PAINT with multiple antibodies binding to ryanodine receptors (RyR) in cardiac tissue sections. **a**: Two populations of secondary antibodies, labelled with extended docking sequences D1 and D5 containing P1 and P5 docking motifs, respectively, bind to single primary antibodies. i, ii: Exchange-PAINT imaging steps with imagers P1 and P5. iii: A strand S1 binds to the extended docking sequence D1, preventing imagers from binding. iv: Strand S2 binds to docking sequence D5 and if in close proximity opens up the S1 loop. This allows imager P1 binding to the S1 docking domain. Bottom: rendered DNA-PAINT images of the respective steps. **b**: Overlay of the DNA-PAINT images described in **a** (P5 yellow, P1 magenta, PD-PAINT cyan). PD-PAINT signal typically only appears where P1 and P5 signals show co-localization (inset). **c:** PD-PAINT with two primary antibodies against RyR. Top: PD-PAINT signal, bottom: overlay of PD-PAINT data (cyan) with P5 (yellow) and P1 (magenta) data of individual secondary antibodies, equivalent to b. Scale bars: 2 µm, inset (b): 500 nm, inset (c): 1 µm.

To confirm that there is negligible interaction between imagers and isolated S1 constructs with a closed loop, beads functionalized with S1 but lacking S2 were imaged (Fig. 3e-h). No DNA-PAINT signal is observed, consistent with the simulation results which indicated that binding events of imagers to the closed loop on S1 are extremely brief and thus undetectable (Fig. 2b and Table S4). Indeed, hardly any binding is observed, even at high imager concentrations (Fig. 3h).

Fig. 4 demonstrates the applicability of PD-PAINT to biological samples, using fixed cardiac muscle tissue. In these experiments, binding sites for S1 and S2 are generated by means of a primary antibody (AB), of mouse origin, targeted against the cardiac ryanodine receptor (RyR2, a large ion channel). This primary AB has been previously used for DNA-PAINT imaging of RyRs [4]. Constructs S1 and S2 were hosted by two different populations of secondary ABs, targeting the mouse primary AB. By simultaneously applying equal concentrations of S1- and S2-conjugated secondary ABs to samples labelled with the primary, we achieved a high proportion of primary ABs featuring S1-S2 pairs. With the epitopes on the same primary antibody providing proximal binding sites, this scenario resembles the one validated in Fig. 3 with streptavidin, albeit now in a complex biological tissue. In order to allow the sequential imaging of all targets involved and to also study the equilibration time of PD-PAINT while imaging, S1 and S2 were not directly conjugated to the secondary ABs. Instead, extended docking sequences D1 and D5, that would later anchor the S1 and S2 strands, respectively, were attached to the secondary ABs. D1 and D5 were designed to respectively bind the modified S1 and S2 constructs with high affinity, resulting in effectively irreversible attachment. The two secondary antibodies were initially imaged (Fig. 4a i+ii) in conventional Exchange-PAINT mode [23], with P1 and P5 imagers binding transiently to D1 and D5, respectively, which host docking domains for these imagers. The good overlap between D1 and D5 images (Fig. 4a i+ii bottom panels) suggests that a high proportion of primary ABs were labelled with both types of secondary ABs. When strand S1 was added (100 nM), while imager P1 was still present, the binding rate for imager P1 was eventually reduced to background levels (Fig. S4c), because S1 permanently hybridizes with D1, blocking the docking site (Fig. 3a iii). Notably, during this step the P1 docking site of S1 remained inaccessible due to the closed stem loop structure. The suppression of DNA-PAINT binding occurred rapidly, within <10 min, which indicates quickly saturating binding of S1 strands to D1 (Fig. S4c). When added in solution, S2 attached with a similarly high rate to D5 (monitored with imager P5, Fig. S4d). Since pairs of ABs labelled with D1 and D5 are located within close distance of each other, once S1 and S2 constructs are both present the stem loop structure on S1 is expected to open with significant probability, enabling the detection of a DNA-PAINT signal by means of imager P1. This is indeed confirmed in Fig. 4a iv. After addition of S1 and S2, a stationary DNA-PAINT binding rate was reached after approx. 30 min, indicating that an equilibrium state of S1-S2 complex formation was reached (see also Fig. S4a,b).

Comparison of the three channels representing the localization of ABs carrying S1, ABs carrying S2 and the PD-PAINT signal, respectively, shows that PD-PAINT signal is only observed in areas of co-localization of the two conventional DNA-PAINT channels, as shown by the overlaid images in Fig. 4b. Note that the limited resolution of conventional DNA-PAINT in complex tissue samples such as the one utilized here, especially along the optical axis (several 100 nm in regular 2D SMLM imaging), is expected to lead to a non-negligible number of false positive co-localization signals. PD-PAINT offers a route to rule out false positives while retaining super-resolved spatial information on the distribution of proximity pairs.

Fig. 4c demonstrates the application of PD-PAINT to detect the proximity of two different epitopes on RyRs in a tissue section, (for additional detail see Fig. S1). The two epitopes were first targeted by two distinct primary ABs, one rabbit-raised and the other mouse-raised. Secondary ABs conjugated to the D1 and D5 strands were then applied, targeting the two different primary ABs, before adding the constructs S1 and S2 to implement PD-PAINT.

The results of PD-PAINT experiments were broadly consistent with those where S1 and S2 carrying secondary ABs were attached to the same primary antibody (Fig. 4a,b), however, here a lower rate of imager binding was detected after equilibration. With the binding rate being proportional to the number of available docking sites [22], the reduced rate indicates a lower number of S1-S2 dimerized pairs. This is consistent with the labelling system used in this approach where S1 and S2 are linked via two sets of antibodies to the protein of interest resulting in an increased average separation, as compared to the situation in Fig. 3a. As supported by MC simulations (Fig. 2a), a greater separation reduces the dimerization probability and thus the fraction of open S1 loops and available docking sites.

The steep dependency of PD-PAINT signals on the proximity of S1 and S2 is further demonstrated in an experiment that serves as a negative control (Fig. S2). For this experiment, collagen type VI (ColVI) and RyR were labelled with primary and secondary antibodies to host D1/S1 and D5/S2 constructs, respectively (Fig. S2a). RyR and ColVI have a broadly similar distribution pattern in cardiomyocytes but are separated by the cell membrane and thus not in direct molecular contact. When the two antibody populations were individually imaged using conventional DNA-PAINT targeted towards the D1 and D5 docking strands (Fig. S2b,c), the resulting two-color DNA-PAINT image exhibited overlap in some areas, an occurrence that would be interpreted as molecular colocalization (Fig. S2d). When the same areas were imaged using PD-PAINT targeting S1 and S2, now tethered to D1 and D5, no PD-PAINT signal was detected above background levels (Fig. S2e). This suggests that the areas of overlap observed in the two-color DNA-PAINT image are false positives and that no epitopes of ColVI and RyR are located within close proximity to each other. This is consistent with the expected distribution of collagen and RyRs - although relative distances can often be as small as ~100 nm, ColVI and RyR would be expected to be separated by 30 nm or more based on myocyte ultrastructure determined by electron microscopy [36]. Note that the probability of S1-S2 dimerization predicted by MC simulations at such separations is, consistently, negligibly small (Fig. 2a), even if taking into account a possibly reduced distance of the proximity probes due to the length of anchoring double strand D1 and the spatial extent of antibody labels (which can account for up to ~20 nm).

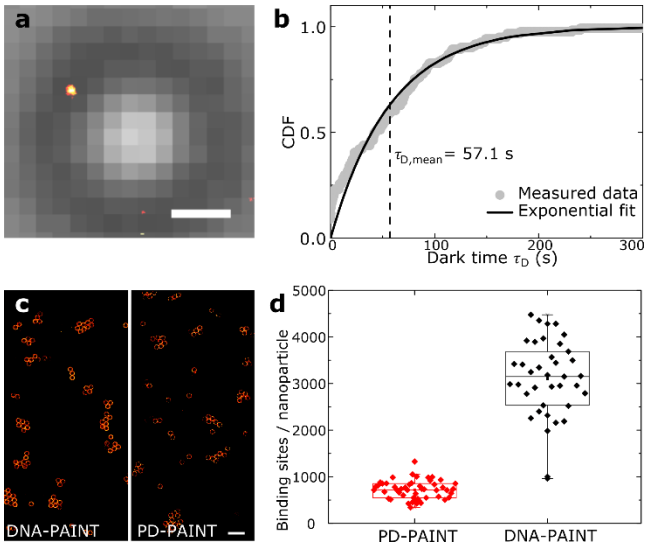

Figure 5. Quantitative imaging with PD-PAINT. **a:** Widefield image of a streptavidin-coated particle (grey), with rendered DNA-PAINT image of a single biotinylated docking strand (yellow), used for qPAINT calibration. **b:** Mean dark times $\tau_{D,\,mean}^{single}$ calculated by fitting an exponential to the cumulative dark time distribution of the calibration site shown in **a**, for a single conventional DNA-PAINT docking site. **c:** Colloidal particles coated with conventional P1 docking strands (left) and PD-PAINT strands S1 and S2. **d:** Using the calibrations obtained in b, the number of accessible docking sites for PD-PAINT (red) and conventional DNA-PAINT (black) per particle is calculated. A reduction of available sites in PD-PAINT compared to conventional DNA-PAINT is expected, due to the stochastic distribution of S1/S2 pairs. Scale bars: 250 nm (a), 2 µm (c).

Exploiting one of the advantages of DNA-PAINT, we show the possibility to quantitatively measure the number of accessible docking sites, and thus the number of protein pairs, from PD-PAINT data. This is done by applying the qPAINT method, previously demonstrated for conventional DNA-PAINT [22]. Quantitative estimates of protein-pair numbers are critical, for example, in assays that test for changes in protein-protein signaling in response to experimental interventions. Some types of proximity detection have been shown to be prone to saturation which can preclude detecting changes in such experiments [37]. To validate quantitative PD-PAINT, biotin-binding sites on streptavidin-coated particles were imaged as discussed above (Fig. 3). In qPAINT, the number of available binding sites within an area of interest is estimated from the kinetics of imager-docking binding events recorded within the area as $N_{bind} = \left(k_{on} \times c_i \times \tau_{D,\,mean}\right)^{-1}$, where k_{on} is the imager-docking association rate, c_i is the imager concentration and $\tau_{D,\,mean}$ is the average time between consecutive binding events, or "mean dark time", determined as discussed in the Supporting Information. Here, k_{on} is estimated from a calibration measurement performed on a bead featuring a single binding site as $k_{on} = \left(\tau_{D,\,mean}^{single} \times c_i\right)^{-1}$ (Fig. 5a) [22]. Binding of a single docking strand on a particle was achieved by functionalizing the particles with a very dilute solution of docking strands (0.5 nM, see also Delcanale et al. [35]). Using $c_i = 5$ nM we obtained $\tau_{D,\,mean}^{single}$ = 57.1 s (Fig. 5b, see Methods in the Supporting Information) and $k_{on} = 3.5 \times 10^6 M^{-1}s^{-1}$ for conventional DNA-PAINT, in broad agreement with previously reported values [35,38].

qPAINT was first applied to a conventional DNA-PAINT experiment performed on beads simply decorated with the P1 docking sequence (black points in Fig. 5d). For PD-PAINT, the experiment was repeated with beads featuring S1 and S2 as described above (red points in Fig. 5d). A reduction of detected PD-PAINT sites as compared to the maximal capacity of biotin binding sites as measured by conventional DNA-PAINT was observed. Such a decrease is expected due to at least three factors: (1) two biotin-binding sites, one occupied by S1 and the other by S2 are required to produce a single docking strand, resulting in a 50% decrease, (2) among the pairs of binding sites the stochastic distribution of strands S1 and S2 reduces the number of S1-S2 pairs as compared to S1-S1 and S2-S2 to ~50% - 63% [39] of the total, corresponding to between 2 to 4 adjacent biotin binding sites being available for S1/S2 binding on a single streptavidin molecule. (3) Finally, we need to consider that ~50% of proximal S1-S2 pairs are dimerized when separated by ~2 nm. Cumulatively, this would reduce the available imager binding sites to ~13-16% of those observed with conventional DNA-PAINT. We measured ~23±9%, in broad agreement with these considerations.

The considerations above show that when combining qPAINT with PD-PAINT, the estimation of the number of all proximal S1-S2 pairs is subject to the knowledge of the distance-dependent P1-P2 dimerization probability. The most precise estimates can thus be obtained in cases where the distance between target epitopes is uniform throughout the sample or approximately known a priori, as for the case of biotin binding sites on streptavidin or proteins clustering in specific morphologies. In cases in which a broad distribution of epitope-distances is expected, as for example, in the case of non-specific and random aggregates, our technique can provide a lower bound to the number of pairs, assuming a peak S1-S2 dimerization probability of 60% (Fig. 2a).

As a final application, we show that, using the vast combinatorial space of DNA-sequence design, it is possible to design orthogonal imaging probes that analogously to S1 and S2 expose different docking strands when in close proximity. Fig. S3 demonstrates the use of spectral and temporal multiplexing to detect two different proximity-pair populations in the same sample. Based on this principle, a virtually unlimited number of distinct protein pairs can be detected within a single sample.

Conclusion. In conclusion, we present Proximity-Dependent PAINT, a technique which allows imaging of the distribution of protein pairs, or other biological targets in close proximity, with nanoscale resolution. As opposed to conventional multi-channel-imaging colocalization techniques, proximity detection is decoupled from the imaging resolution, which is especially important in biological cell and tissue samples where the achievable resolution can vary greatly due to refractive index inhomogeneities and related optical challenges. Indeed, with PD-PAINT the proximity range can be smaller than the imaging resolution which is a distinct advantage. A similar decoupling from imaging resolution can be achieved by a FRET-based assay, a fluorescent method that is distance sensitive in the nanometer range [40]. However, in contrast to FRET, PD-PAINT does not require specific dye pairs, eliminates the need for a more complex excitation and detection setup, and does not suffer from the effects of specific molecular orientations which can complicate the interpretation of FRET experiments. In addition, PD-PAINT can be efficiently multiplexed, a more challenging task with FRET based approaches.

We show that PD-PAINT is compatible with the complexities of biological environments by imaging different epitopes of primary antibodies and different epitopes of the ryanodine receptor, a large protein, in fixed cardiac tissue sections. Owing to the modularity of the DNA nanostructures used, PD-PAINT can be implemented relatively easily and with little penalty as an additional step in any Exchange-PAINT experiment [21]. With modern sensitive and affordable cameras (Exchange-) PD-PAINT is straightforward to implement on a conventional fluorescence microscope, the equipment required can be assembled from components with a relatively modest budget [41]. Additionally, the technique can be adapted to various marker types by conjugating the proximity-detection strands S1 and S2 directly to secondary antibodies, primary antibodies, aptamers and related emerging marker technologies.

Guided by quantitative numerical calculations, one could foresee design changes to the basic PD-PAINT machinery aimed at optimizing its performance in specific experimental settings. For example, one could fine tune the range of proximity-detectability. The PD-PAINT system could also be modified to sense the proximity of more than two targets, similarly to what has been previously shown for PLA [42].

Increasing the affinity between the imager and the S1 docking domain, e.g. by adjusting the CG/AT ratio or by extending the number of bases in the stem loop, in combination with an adjusted imager concentration, would enable a near-permanent labelling of open S1-loop structures with single imagers. In this configuration, the PD-PAINT machinery can be exploited to render other super-resolution imaging modalities proximity sensitive, such as STED, SIM, (d)STORM, (f)PALM, or even widefield and confocal microscopy [12,13,15,16,18].

Supporting Information. Materials and experimental methods, simulation methods, tables showing sampling windows used in the simulation, a table showing DNA sequences, a table showing expected half-lives of imager binding, a figure showing a detailed view of PD-PAINT using two primary antibodies, a figure showing a negative control experiment for PD-PAINT, a figure showing multiplexed PD-PAINT imaging, a figure showing the equilibration time of S1/S2 interaction.

Corresponding Author

* Christian Soeller
Living Systems Institute
University of Exeter
Exeter
EX4 4QD
UNITED KINGDOM
Email: C.Soeller@exeter.ac.uk
Telephone: +44 (0)1392 726608
Fax: +44 (0)1392 217965

Author Contributions. The manuscript was written through contributions of all authors.

Funding Sources. This work was supported by the Human Frontier Science Program (No. 0027/2013) and the Engineering and Physical Sciences Research Council of the UK (No. EP/N008235/1) and Biotechnology and Biological Sciences Research Council Grant BB/P026508/1. L.D.M. acknowledges support from the Royal Society through a University Research Fellowship (UF160152). W.T.K. acknowledges support from an EPSRC DTP studentship.

Conflict of Interest Disclosure. T.L., W.T.K., A.H.C., L.D.M. and C.S. are inventors on patent application GB1904095.5.

Acknowledgment. We thank Dr Ruisheng Lin for assistance with the imaging setup.

References

(1) Jones, S.; Thornton, J. M. Principles of Protein-Protein Interactions. PNAS **1996**, 93 (1), 13–20. https://doi.org/10.1073/pnas.93.1.13.
(2) Phizicky, E. M.; Fields, S. Protein-Protein Interactions: Methods for Detection and Analysis. Microbiol Rev **1995**, 59 (1), 94–123.
(3) Fields, S.; Song, O. A Novel Genetic System to Detect Protein-Protein Interactions. Nature **1989**, 340 (6230), 245–246. https://doi.org/10.1038/340245a0.
(4) Jayasinghe, I.; Clowsley, A. H.; Lin, R.; Lutz, T.; Harrison, C.; Green, E.; Baddeley, D.; Michele, L. D.; Soeller, C. True Molecular Scale Visualization of Variable Clustering Properties of Ryanodine Receptors. Cell Reports **2018**, 22 (2), 557–567. https://doi.org/10.1016/j.celrep.2017.12.045.
(5) Söderberg, O.; Gullberg, M.; Jarvius, M.; Ridderstråle, K.; Leuchowius, K.-J.; Jarvius, J.; Wester, K.; Hydbring, P.; Bahram, F.; Larsson, L.-G.; et al. Direct Observation of Individual Endogenous Protein Complexes in Situ by Proximity Ligation. Nature Methods **2006**, 3 (12), 995–1000. https://doi.org/10.1038/nmeth947.
(6) Fredriksson, S.; Gullberg, M.; Jarvius, J.; Olsson, C.; Pietras, K.; Gústafsdóttir, S. M.; Östman, A.; Landegren, U. Protein Detection Using Proximity-Dependent DNA Ligation Assays. Nature Biotechnology **2002**, 20 (5), 473–477. https://doi.org/10.1038/nbt0502-473.
(7) Gullberg, M.; Gústafsdóttir, S. M.; Schallmeiner, E.; Jarvius, J.; Bjarnegård, M.; Betsholtz, C.; Landegren, U.; Fredriksson, S. Cytokine Detection by Antibody-Based Proximity Ligation. PNAS **2004**, 101 (22), 8420–8424. https://doi.org/10.1073/pnas.0400552101.
(8) Söderberg, O.; Leuchowius, K.-J.; Gullberg, M.; Jarvius, M.; Weibrecht, I.; Larsson, L.-G.; Landegren, U. Characterizing Proteins and Their Interactions in Cells and Tissues Using the in Situ Proximity Ligation Assay. Methods **2008**, 45 (3), 227–232. https://doi.org/10.1016/j.ymeth.2008.06.014.
(9) Dirks, R. M.; Pierce, N. A. Triggered Amplification by Hybridization Chain Reaction. PNAS **2004**, 101 (43), 15275–15278. https://doi.org/10.1073/pnas.0407024101.
(10) Koos, B.; Cane, G.; Grannas, K.; Löf, L.; Arngården, L.; Heldin, J.; Clausson, C.-M.; Klaesson, A.; Hirvonen, M. K.; de Oliveira, F. M. S.; et al. Proximity-Dependent Initiation of Hybridization Chain Reaction. Nature Communications **2015**, 6, 7294. https://doi.org/10.1038/ncomms8294.
(11) Koos, B.; Andersson, L.; Clausson, C.-M.; Grannas, K.; Klaesson, A.; Cane, G.; Söderberg, O. Analysis of Protein Interactions in Situ by Proximity Ligation Assays. In High-Dimensional Single Cell Analysis: Mass Cytometry, Multi-parametric Flow Cytometry and Bioinformatic Techniques; Fienberg, H. G., Nolan, G. P., Eds.; Current Topics in Microbiology and Immunology; Springer Berlin Heidelberg: Berlin, Heidelberg, 2014; pp 111–126. https://doi.org/10.1007/82_2013_334.
(12) Bailey, B.; Farkas, D. L.; Taylor, D. L.; Lanni, F. Enhancement of Axial Resolution in Fluorescence Microscopy by Standing-Wave Excitation. Nature **1993**, 366 (6450), 44–48. https://doi.org/10.1038/366044a0.
(13) Hell, S. W.; Wichmann, J. Breaking the Diffraction Resolution Limit by Stimulated Emission: Stimulated-Emission-Depletion Fluorescence Microscopy. Optics letters **1994**, 19 (11), 780–782.
(14) Klar, T. A.; Jakobs, S.; Dyba, M.; Egner, A.; Hell, S. W. Fluorescence Microscopy with Diffraction Resolution Barrier Broken by Stimulated Emission. PNAS **2000**, 97 (15), 8206–8210. https://doi.org/10.1073/pnas.97.15.8206.
(15) Betzig, E.; Patterson, G. H.; Sougrat, R.; Lindwasser, O. W.; Olenych, S.; Bonifacino, J. S.; Davidson, M. W.; Lippincott-Schwartz, J.; Hess, H. F. Imaging Intracellular Fluorescent Proteins at Nanometer Resolution. Science **2006**, 313 (5793), 1642–1645. https://doi.org/10.1126/science.1127344.
(16) Hess, S. T.; Girirajan, T. P. K.; Mason, M. D. Ultra-High Resolution Imaging by Fluorescence Photoactivation Localization Microscopy. Biophysical Journal **2006**, 91 (11), 4258–4272. https://doi.org/10.1529/biophysj.106.091116.
(17) Rust, M. J.; Bates, M.; Zhuang, X. Sub-Diffraction-Limit Imaging by Stochastic Optical Reconstruction Microscopy (STORM). Nature Methods **2006**, 3 (10), 793–796. https://doi.org/10.1038/nmeth929.
(18) Heilemann, M.; van de Linde, S.; Schüttpelz, M.; Kasper, R.; Seefeldt, B.; Mukherjee, A.; Tinnefeld, P.; Sauer, M. Subdiffraction-Resolution Fluorescence Imaging with Conventional Fluorescent Probes. Angewandte Chemie International Edition **2008**, 47 (33), 6172–6176. https://doi.org/10.1002/anie.200802376.
(19) Schnitzbauer, J.; Strauss, M. T.; Schlichthaerle, T.; Schueder, F.; Jungmann, R. Super-Resolution Microscopy with DNA-PAINT. Nat. Protocols **2017**, 12 (6), 1198–1228. https://doi.org/10.1038/nprot.2017.024.
(20) Xu, K.; Babcock, H. P.; Zhuang, X. Dual-Objective STORM Reveals Three-Dimensional Filament Organization in the Actin Cytoskeleton. Nature Methods **2012**, 9 (2), 185–188. https://doi.org/10.1038/nmeth.1841.
(21) Dai, M.; Jungmann, R.; Yin, P. Optical Imaging of Individual Biomolecules in Densely Packed Clusters. Nature Nanotechnology **2016**, 11 (9), 798–807. https://doi.org/10.1038/nnano.2016.95.
(22) Jungmann, R.; Avendaño, M. S.; Dai, M.; Woehrstein, J. B.; Agasti, S. S.; Feiger, Z.; Rodal, A.; Yin, P. Quantitative Super-Resolution Imaging with QPAINT. Nat Meth **2016**, 13 (5), 439–442. https://doi.org/10.1038/nmeth.3804.
(23) Jungmann, R.; Avendaño, M. S.; Woehrstein, J. B.; Dai, M.; Shih, W. M.; Yin, P. Multiplexed 3D Cellular Super-Resolution Imaging with DNA-PAINT and Exchange-PAINT. Nat Meth **2014**, 11 (3), 313–318. https://doi.org/10.1038/nmeth.2835.
(24) Li, F.; Tang, Y.; Traynor, S. M.; Li, X.-F.; Le, X. C. Kinetics of Proximity-Induced Intramolecular DNA Strand Displacement. Anal. Chem. **2016**, 88 (16), 8152–8157. https://doi.org/10.1021/acs.analchem.6b01900.

(25) Genot, A. J.; Zhang, D. Y.; Bath, J.; Turberfield, A. J. Remote Toehold: A Mechanism for Flexible Control of DNA Hybridization Kinetics. J. Am. Chem. Soc. **2011**, 133 (7), 2177–2182. https://doi.org/10.1021/ja1073239.
(26) Srinivas, N.; Ouldridge, T. E.; Šulc, P.; Schaeffer, J. M.; Yurke, B.; Louis, A. A.; Doye, J. P. K.; Winfree, E. On the Biophysics and Kinetics of Toehold-Mediated DNA Strand Displacement. Nucleic Acids Res **2013**, 41 (22), 10641–10658. https://doi.org/10.1093/nar/gkt801.
(27) Ouldridge, T. E.; Louis, A. A.; Doye, J. P. K. DNA Nanotweezers Studied with a Coarse-Grained Model of DNA. Phys. Rev. Lett. **2010**, 104 (17), 178101. https://doi.org/10.1103/PhysRevLett.104.178101.
(28) Ouldridge, T. E.; Louis, A. A.; Doye, J. P. K. Structural, Mechanical, and Thermodynamic Properties of a Coarse-Grained DNA Model. J. Chem. Phys. **2011**, 134 (8), 085101. https://doi.org/10.1063/1.3552946.
(29) Pettersen, E. F.; Goddard, T. D.; Huang, C. C.; Couch, G. S.; Greenblatt, D. M.; Meng, E. C.; Ferrin, T. E. UCSF Chimera--a Visualization System for Exploratory Research and Analysis. J Comput Chem **2004**, 25 (13), 1605–1612. https://doi.org/10.1002/jcc.20084.
(30) Zadeh, J. N.; Steenberg, C. D.; Bois, J. S.; Wolfe, B. R.; Pierce, M. B.; Khan, A. R.; Dirks, R. M.; Pierce, N. A. NUPACK: Analysis and Design of Nucleic Acid Systems. Journal of Computational Chemistry **2011**, 32 (1), 170–173. https://doi.org/10.1002/jcc.21596.
(31) Mognetti, B. M.; Leunissen, M. E.; Frenkel, D. Controlling the Temperature Sensitivity of DNA-Mediated Colloidal Interactions through Competing Linkages. Soft Matter **2012**, 8 (7), 2213–2221. https://doi.org/10.1039/C2SM06635A.
(32) Parolini, L.; Mognetti, B. M.; Kotar, J.; Eiser, E.; Cicuta, P.; Di Michele, L. Volume and Porosity Thermal Regulation in Lipid Mesophases by Coupling Mobile Ligands to Soft Membranes. Nat Commun **2015**, 6, 5948. https://doi.org/10.1038/ncomms6948.
(33) Hendrickson, W. A.; Pähler, A.; Smith, J. L.; Satow, Y.; Merritt, E. A.; Phizackerley, R. P. Crystal Structure of Core Streptavidin Determined from Multiwavelength Anomalous Diffraction of Synchrotron Radiation. PNAS **1989**, 86 (7), 2190–2194. https://doi.org/10.1073/pnas.86.7.2190.
(34) Lutz, T.; Clowsley, A. H.; Lin, R.; Pagliara, S.; Michele, L. D.; Soeller, C. Versatile Multiplexed Super-Resolution Imaging of Nanostructures by Quencher-Exchange-PAINT. Nano Res. **2018**, 1–14. https://doi.org/10.1007/s12274-018-1971-6.
(35) Delcanale, P.; Miret-Ontiveros, B.; Arista-Romero, M.; Pujals, S.; Albertazzi, L. Nanoscale Mapping Functional Sites on Nanoparticles by Points Accumulation for Imaging in Nanoscale Topography (PAINT). ACS Nano **2018**, 12 (8), 7629–7637. https://doi.org/10.1021/acsnano.7b09063.
(36) Morita, T.; Shimada, T.; Kitamura, H.; Nakamura, M. Demonstration of Connective Tissue Sheaths Surrounding Working Myocardilal Cells and Purkinje Cells of the Sheep Moderator Band. Arch. Histol. Cytol. **1991**, 54 (5), 539–550. https://doi.org/10.1679/aohc.54.539.
(37) Mocanu, M.-M.; Váradi, T.; Szöllősi, J.; Nagy, P. Comparative Analysis of Fluorescence Resonance Energy Transfer (FRET) and Proximity Ligation Assay (PLA). PROTEOMICS **2011**, 11 (10), 2063–2070. https://doi.org/10.1002/pmic.201100028.
(38) Jungmann, R.; Steinhauer, C.; Scheible, M.; Kuzyk, A.; Tinnefeld, P.; Simmel, F. C. Single-Molecule Kinetics and Super-Resolution Microscopy by Fluorescence Imaging of Transient Binding on DNA Origami. Nano Lett. **2010**, 10 (11), 4756–4761. https://doi.org/10.1021/nl103427w.
(39) Li, F.; Zhang, H.; Wang, Z.; Li, X.; Li, X.-F.; Le, X. C. Dynamic DNA Assemblies Mediated by Binding-Induced DNA Strand Displacement. J. Am. Chem. Soc. **2013**, 135 (7), 2443–2446. https://doi.org/10.1021/ja311990w.
(40) Truong, K.; Ikura, M. The Use of FRET Imaging Microscopy to Detect Protein–Protein Interactions and Protein Conformational Changes in Vivo. Current Opinion in Structural Biology **2001**, 11 (5), 573–578. https://doi.org/10.1016/S0959-440X(00)00249-9.
(41) Ma, H.; Fu, R.; Xu, J.; Liu, Y. A Simple and Cost-Effective Setup for Super-Resolution Localization Microscopy. Scientific Reports **2017**, 7 (1), 1542. https://doi.org/10.1038/s41598-017-01606-6.
(42) Schallmeiner, E.; Oksanen, E.; Ericsson, O.; Spångberg, L.; Eriksson, S.; Stenman, U.-H.; Pettersson, K.; Landegren, U. Sensitive Protein Detection via Triple-Binder Proximity Ligation Assays. Nature Methods **2007**, 4 (2), 135–137. https://doi.org/10.1038/nmeth974.